Heliyon 9 (2023) e18636

Contents lists available at ScienceDirect

Heliyon

journal homepage: www.cell.com/heliyon

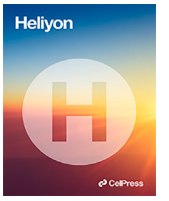

Research article

Further developments of the extended quadrature method of moments to solve population balance equations

Meltem Turan [a], Abhishek Dutta [b,*]

[a] Ege University, Department of Mathematics, Izmir 35180, Turkey
[b] Izmir Institute of Technology, Department of Chemical Engineering, Gülbahçe Campus, Izmir 35430, Turkey

ARTICLE INFO

Meltem Turan would like to dedicate the work in the memory of her mother Nevin Turan who passed away untimely while preparing this study

Keywords:
Moment-inversion procedure
Halley-Ridder method
Extended quadrature method of moments
Population balance equation

ABSTRACT

Developing numerical methods to solve polydispersed flows using a Population Balance Equation (PBE) is an active research topic with wide engineering applications. The Extended Quadrature Method of Moments (EQMOM) approximates the number density as a positive mixture of Kernel Density Functions (KDFs) that allows physical source terms in the PBEs to compute continuous or point-wise form according to the moments. The moment-inversion procedure used in EQMOM has limitations such as the inability to calculate certain roots even if it is defined, absence of consistent result when multiple roots exist or when the roots are nearly equal. To address these limitations, the study proposes a modification of the moment-inversion procedure to solve the PBE based on the proposed Halley-Ridder (H-R) method. Although there is no significant improvement in the extent of variability relative to the mean of the tested shape parameter σ values, an increase in the number of floating point operations (FLOPS) is observed which the proposed algorithm responds in limitations mentioned above. The total number of FLOPS for all the kernels used for the approximation increased by around 30%. This is an improvement towards the development of a more reliable and robust moment-inversion procedure.

1. Introduction

Population Balance Model (PBM) is ubiquitous in industrial applications where multiple phases are involved. For instance, PBM is applied in the modeling of gas–liquid [1], gas-solid [2] and gas-solid-liquid [3] phases with applications in aerosol technology [4], petrochemical technology [5], crystallization technology [6] and fermentation technology[7] to name a few. Population balance is a transport equation that is used to track the dynamics of the evolving particulate phase Number Density Function (NDF) with a given set of internal coordinates (e.g. size, area, shape or chemical composition) in the physical as well as the phase space. The density function depends on time t, spatial position x and internal coordinates ξ. A typical Population Balance Equation (PBE) includes growth terms on individual particles, source terms for the formation of new particles, and aggregation and breakage terms involving multiple particles. In this study, only one internal coordinate representing size in terms of particle radius or volume ($\xi \equiv r$ or v) is considered.

To solve the PBE, there are different solution approaches in literature, such as lattice Boltzmann method [7,8], sectional method [9,10] and homotopy method [10,11]. A critical review that provides a comprehensive analysis of the state of the art in numerical approaches with emphasis in algorithmic details and their applications for solving PBEs can be found in Singh et al.[12]. Most of the

* Corresponding author at: Department of Chemical Engineering, Izmir Institute of Technology, Gülbahçe Campus, Izmir 35430, Turkey.
E-mail address: abhishekdutta@iyte.edu.tr (A. Dutta).

https://doi.org/10.1016/j.heliyon.2023.e18636
Received 8 June 2023; Received in revised form 18 July 2023; Accepted 24 July 2023

Available online 28 July 2023

numerical approaches mentioned in [12] have limitations such as high computational cost. A popular solution approach is using the method of moments, which is both robust and reliable for solving PBEs. A class of such methods solves the moments, for example the quadrature-based methods have been used. However, when discrete values of NDF are needed, they are not directly obtained from the moments such as in Quadrature Method of Moments (QMOM). To overcome this, the Extended Quadrature Method of Moments (EQMOM) was proposed by Yuan et al. [13]. EQMOM approximates the NDF from its moments as a positive mixture of Kernel Density Function (KDF) of the same parametric family. The reconstruction can be done for a very realisable moment set, except reproducing the last moment. In the moment-inversion procedure of Yuan et al. [13], both Ridder's method [14] and bounded Secant method were employed to update shape parameter of approximation in [13]. Nguyen et al. [15] improved the moment-inversion procedure which gives a response for cases in which the moments are weakly realisable. Pigou et al. [16] improved the numerical aspects of EQMOM significantly by reducing the computational cost of this method's core iterative procedure, however with some exceptions. They constructed the procedure using Ridder's method which uses two values to shrink the interval according to the sign of functions. In Pigou et al. [16], the initial interval was determined by observation of recurring coefficients. However, as a detailed mathematical proof of these observations have not been given in their study there is a possibility that the root can be out of the initial interval i.e., they cannot calculate the root (i) out of the initial interval, (ii) when the roots of the function are nearly equal, and (iii) when there is a gap where the convergence criteria is not defined. Although these cases (i), (ii) and (iii) are not frequently encountered in moment sets, it is necessary to propose a more robust algorithm that responds to all possible scenarios.

The need for a fast and numerically efficient algorithm to solve the ill-conditioned moment problem through a robust moment-inversion procedure becomes prominent when external features like turbulent flow properties [17], dilute gas-particle flows [18] and reacting-mixing species [19] play an important role for any chemical process under investigation. The present study focuses on the improvement of the moment-inversion procedure for three special cases which do not yield satisfactory results and are examined in detail. To overcome the first two shortcomings, the procedure given in Pigou et al. [16] is modified. The modified procedure combines the most desirable properties of Halley's method [20] which finds the root of one variable function that has continuous second derivative and whose convergence is not guaranteed with Ridder's method which finds the root of a continuous function and whose convergence is guaranteed. In this study, Halley's method is used by substituting Newton's forward difference method instead of the derivatives. To reach the root being out of the interval and not to skip the small interval where the sign of the function changes, Halley's approach point is calculated by using Ridder's approach point. The combination of these two methods is proposed as the Halley-Ridder (H-R) method in this study. In this method, the initial interval is taken as $[0,1]$. The method responds for cases (i) and (ii) but does not respond for case (iii). This is because the convergence criteria depends not only on the sign of functions but also on the limitation of the functions to the one for the Hausdorff problem. It is difficult to cross the gap where the convergence criteria is not defined and reach the root after this gap. Therefore, when no root is found in the initial interval $[0,1]$, the additional condition of searching the root for the interval $[1,\sigma_2]$ is added to the procedure, where σ_2 is the analytic solution of the function for $i=2$, which is obtained by Chebyshev algorithm. In this study, the H-R method is applied to a lot of moment sets taken from literature. The root is out of the initial interval $[0,1]$ for some of the tested moment vectors and this was calculated without encountering any problem. More than one root exist for some of the tested moment vectors and the lowest root among them was calculated by the H-R method. So small changes in raw moments will cause minor changes in the resulting shape parameter values. Furthermore, due to the additional condition mentioned earlier, the root can be calculated for case (iii) which indicates a greater applicability of the proposed method.

2. Population Balance Equation (PBE)

Population balance is a continuity equation based on Number Density Function (NDF). This function is defined depending on the properties of the evolution of the particle population under observation. Considering the coordinates of the property vector $\xi \equiv (\xi_1, \xi_2, \ldots, \xi_n)$ which specify the state of the particle, the NDF $\eta(\xi; x, t)$ is defined as

$$\eta(\xi_1, \xi_2, \ldots, \xi_n; x, t) d\xi_1, d\xi_2, \ldots, d\xi_n = \eta(\xi; x, t) d\xi$$

and represents the number of particles with a value of the property vector between ξ and $\xi + d\xi$. The function $\eta(\xi, t)$ can have only one internal coordinate such as particle radius or volume, or multiple internal coordinates such as particle volume and particle shape. In this study, a number density function (NDF) is defined in terms of particle radius or volume ($\xi_1 \equiv r$ or v) and the homogeneous population balance equation (PBE) is represented as

$$\frac{\partial \eta(t,\xi)}{\partial t} + \frac{\partial}{\partial \xi}[g(t,\xi)\eta(t,\xi)] = B_{agg}(t,\xi) - D_{agg}(t,\xi) + B_{br}(t,\xi) - D_{br}(t,\xi). \tag{1}$$

The aggregation terms are given by

$$B_{agg}(t,\xi) = \frac{1}{2}\int_{\xi_{min}}^{\xi} \beta(t, \xi - \xi', \xi')\eta(t, \xi - \xi')\eta(t, \xi')d\xi' \tag{2}$$

and

$$D_{agg}t,\xi) = \int_{\xi_{min}}^{\xi_{max}} \beta(t,\xi,\xi')\eta(t,\xi)\eta(t,\xi')d\xi', \tag{3}$$

where $\beta(t,\xi,\xi')$ is the aggregation kernel. The breakage terms can be given as

$$B_{br}(t,\xi) = \int_{\xi}^{\xi_{max}} \theta(t,\xi,\xi')b(\xi,\xi')\eta(t,\xi,\xi')d\xi' \tag{4}$$

and

$$D_{br} = \theta(t,\xi,\xi')\eta(t,\xi,\xi'), \tag{5}$$

where $\theta(t,\xi,\xi')$ is breakage kernel and $b(\xi,\xi')$ is the daughter particle distribution function.

3. Background theory

3.1. Quadrature Method of Moments (QMOM)

Let $\mu(\xi)$ defined on a domain space Ω_ξ be a non-decreasing function and $d\mu(\xi)$ induced by $\mu(\xi)$ be a positive metric of this domain space. This metric is related to the number density $\eta(\xi)$ such that $d\mu(\xi) = \eta(\xi)d\xi$. Let $\mathbf{m}_N$ be the vector:

$$\mathbf{m}_N = \begin{bmatrix} m_0 \\ m_1 \\ \vdots \\ m_N \end{bmatrix}, \quad m_k = \int_{\Omega_\xi} \xi^k \eta(\xi)d\xi, \tag{6}$$

whose elements are the first $N+1$ integer moments of this metric. Three domain spaces are considered: (i) $\Omega_\xi = (-\infty,+\infty)$, (ii) $\Omega_\xi = (0,+\infty)$ and (iii) $\Omega_\xi = (0,1)$. For each of these domain spaces, all possible positive metrics defined on Ω_ξ can induce a set of vectors of finite moments $\mathbf{m}_N$ (6) within the associated realisable moment space $M_N(\Omega_\xi)$.

The transport equation for kth order moment is obtained by multiplying the PBE (1), where B_{agg}, D_{agg}, B_{br} and D_{br} are given in (2),(3),(4) and (5) respectively, by ξ^k and integrating over Ω_ξ and can be given as

$$\frac{m_k}{dt} = -g(t,\xi)\eta(t,\xi)|_{\xi_{min}}^{\xi_{max}} + \int_{\xi_{min}}^{\xi_{max}} k\xi^{k-1}g(t,\xi)\eta(t,\xi)d\xi + \int_{\xi_{min}}^{\xi_{max}} \xi^k[B_{agg}(t,\xi) - D_{agg}(t,\xi)]d\xi + \int_{\xi_{min}}^{\xi_{max}} \xi^k[B_{br}(t,\xi) - D_{br}(t,\xi)] + \int_{\xi_{min}}^{\xi_{max}} \xi^k Q(t,\xi)\eta(t,\xi)d\xi. \tag{7}$$

EQMOM is based on QMOM proposed by McGraw [21] which approximates the integral properties of a NDF using only the first few moments of the distribution. Using a Gauss quadrature rule defined as

$$\int_{\Omega_\xi} f(\xi)d\mu(\xi) = \sum_{i=1}^{P} w_i f(\xi_i), \tag{8}$$

where $w_P = [w_1, w_2, ..., w_P]^T$ are weights, $\xi_P = [\xi_1, ..., \xi_P]^T$ are nodes, and it holds true if $f(\xi) = \xi^k$, $\forall k \in 0, 1, ..., 2P-1$ where $P \in \mathbb{N}$. Otherwise, this quadrature rule will calculate the integral approximately. The vectors ξ_P and w_P are computed by tridiagonal Jacobi matrix, which is given by

$$J_n(d\mu) = \begin{bmatrix} a_0 & \sqrt{b_1} & & 0 \\ \sqrt{b_1} & a_1 & \ddots & \\ & \ddots & \ddots & \sqrt{b_{P-1}} \\ 0 & & \sqrt{b_{P-1}} & a_{P-1} \end{bmatrix}, \tag{9}$$

where $\mathbf{a}_{P-1} = [a_0, a_1, \dots, a_{P-1}]^T$ and $\mathbf{b}_{P-1} = [b_1, b_2, \dots, b_{P-1}]^T$ recurring coefficients can be computed by the Quotient-Difference [22], the Product-Difference [23] or the Chebyshev [24] algorithms, such that nodes of ξ_P are eigenvalues of the matrix (9) and the nodes of w_P are $w_i = m_0 v_{1,i}^2$ ($v_{1,i}$ is the first component of the normalized eigenvector corresponding to the eigenvalue ξ_i.

In other words, the Gaussian quadrature computed with QMOM approximates $\eta(\xi)$ as

$$\eta(\xi) = \sum_{i=1}^{P} w_i \delta(\xi, \xi_i), \tag{10}$$

which is a weighted sum of Dirac delta distribution defined by sifting property.

3.2. Extended Quadrature Method of Moments (EQMOM)

For most applications, non-moment integral properties or discrete evaluation of a distribution needs to be calculated. So $\eta(\xi)$ needs to be continuous distribution which is not available in QMOM (see (10)). To tackle this problem, there are various approaches suggested in literature [21,25,26]. One of them is the EQMOM which uses a basis of non-negative Kernel Density Functions (KDFs) in place of Dirac delta functions.

EQMOM approximates $\eta(\xi)$ as a positive combination of KDFs that allow to compute unclosed source terms

$$\tilde{\eta}(\xi) = \sum_{i=1}^{P} w_i \delta_\sigma(\xi, \xi_i), \tag{11}$$

where w_i is the weight of the i-th node, δ_σ is the chosen KDF to perform the approximation where σ is the shape parameter of the approximation and ξ_i is the location variable of i-th node. Standard normalized distribution functions are chosen as the kernels (e.g. Gaussian, Log-normal, Laplace, Weibull, etc.). For consistency, δ_σ is chosen as

$$\lim_{\sigma \to 0} \delta_\sigma(\xi, \xi_i) = \delta(\xi, \xi_i),$$

such that σ is sufficiently small. Thanks to this, EQMOM is numerically stable when a moment set $\mathbf{m}_N$ is on the boundary of realisable moment space. Moreover, integral properties of the NDF can be computed by EQMOM with high accuracy. Approximation of integral terms can be given as

$$\int_{\Omega_\xi} f(\xi)\eta(\xi)d\xi \approx \sum_{i=1}^{P} w_i \left[\int_{\Omega_\xi} f(\xi)\delta_\sigma(\xi, \xi_i)d\xi \right]. \tag{12}$$

There are multiple available variations of EQMOM in literature such as the Gauss EQMOM [27,28], Log-Normal EQMOM [29], and Beta and Gamma EQMOM [13]. Also, the integral given in (12) can be calculated approximately by a quadrature rule.

3.2.1. Log-normal Kernel Density Function (KDF)

Gauss-Wigert quadratures [30] is implemented for the preservation of moments for a Log-normal EQMOM reconstruction:

$$\int_0^\infty f(\xi)\eta(\xi)d\xi \approx \sum_{i=1}^{P} w_i \sum_{j=1}^{Q} \omega_j^{(\sigma)} f(\xi_i \lambda_j^{(\sigma)}) \tag{13}$$

with $\mathbf{w}_P$, ξ_P and σ being the reconstruction parameters calculated from $\mathbf{m}_{2P}$. $\lambda_Q^{(\sigma)}$ are eigenvalues of the Jacobi matrix J_Q whose elements a_k and b_k are calculated by $a_k = ((z^2+1)z^{2k}-1)z^{2k-1}$ and $b_k = (z^{2k}-1)z^{6k-4}$ with $z = exp(\sigma^2/2)$. ω_Q is given by $\omega_j = P_0 v_{1,j}^2$ ($P_0 = 1$) with $v_{1,j}$ being the first component of the normalized eigenvector corresponding to the eigenvalue λ_j.

3.2.2. Gamma Kernel Density Function (KDF)

Gauss-Laguerre quadrature [30] is implemented for preserving the moments for a Gamma EQMOM reconstruction:

$$\int_0^\infty f(\xi)\eta(\xi)d\xi \approx \sum_{i=1}^{P} \frac{w_i}{\Gamma(\frac{\xi_i}{\sigma})} \sum_{j=1}^{Q} \omega_j^{\alpha_i} f(\sigma \lambda_j^{(\alpha_i)}), \tag{14}$$

with $\mathbf{w}$, ξ_P and σ being the reconstruction parameters calculated from m_{2P}. $\lambda_Q^{(\alpha_i)}$ are eigenvalues of the Jacobi matrix J_Q (9) whose elements are $a_0 = 1+\alpha_0$, $a_k = 2 + a_{k-1}$ and $b_k = k(k+\alpha_k)$ with $\alpha_k = \frac{\xi_k}{\sigma} - 1$. $\omega_Q^{(\alpha_i)}$ is given by $\omega_j = P_0 v_{1,j}^2$ ($P_0 = \Gamma(1+\alpha_j)$) with $v_{1,j}$ being the first component of the normalized eigenvector corresponding to the eigenvalue $\lambda_j^{(\alpha_i)}$ with $\alpha_i = \frac{\xi_i}{\sigma} - 1$.

The computation of the weights $w_P = [w_1, w_2, ..., w_P]^T$, the nodes $\xi_P = [\xi_1, ..., \xi_P]^T$ and the shape parameter σ values from the moment set $\mathbf{m}_{2P}$ are calculated by the moment-inversion procedure. The moment-inversion procedures used in literature are mentioned briefly in section 4.1.

4. Moment-inversion procedure

Various numerical strategies [21,13] have been proposed to reduce the dimensionality of the PBE. In standard moment methods, this balance equation is multiplied by a function ξ^k and integrated over Ω_ξ. This approach causes a closure problem where moment transport equations are written in terms of the number of moments higher than the number of transport equations[31]. This problem can be overcome by obtaining the unknown moments in terms of known moments using the transported moment set or reconstructing the NDF from the transported moments from which the unclosed terms can be evaluated.

4.1. Procedures based on moment realisability

For the metric $d\mu(\xi) = \eta(\xi)d\xi$ given by (6) assumes $\mathbf{m}_N$ be the vector of the first $N+1$ integer moments vector of the metric $d\mu(\xi) = \eta(\xi)d\xi$, with $N = 2P$ as an even integer.

The moment-inversion procedure aims to determine the parameters σ, $w_P = [w_1, \dots, w_P]^T$ and $\xi_P = [\xi_1, \dots, \xi_P]^T$ such that $\mathbf{m}_N = \tilde{\mathbf{m}}_N$ with

$$\tilde{\mathbf{m}}_N = \begin{bmatrix} \tilde{m}_0 \\ \tilde{m}_1 \\ \vdots \\ \tilde{m}_N \end{bmatrix}, \quad \tilde{m}_k = \int_{\Omega_\xi} \xi^k \tilde{\eta}(\xi) d\xi, \tag{15}$$

where $\tilde{\eta}(\xi)$ is given in (11). For any value of the shape parameter σ, Yuan et al. [13] proposed a procedure that requires calculation of the parameters w_P and ξ_P such that $\mathbf{m}_{N-1} = \tilde{\mathbf{m}}_{N-1}$, where $\tilde{\mathbf{m}}_{N-1}$ is given in (15). This simplifies the moment-inversion problem to a scalar non-linear equation by searching for a root function $D_N(\sigma) = m_N - \tilde{m}_N(\sigma)$. For the KDFs used in EQMOM, using the approach developed by Yuan et al. [13] and improved by Nguyen et al. [15], the following linear system can be written as:

$$\tilde{\mathbf{m}}_n = A_n(\sigma).\mathbf{m}_n^*, \tag{16}$$

where $A_n(\sigma)$ is a lower-triangular $(n+1)\times(n+1)$ matrix. The elements of this matrix depend on chosen KDF and σ. The moments $\mathbf{m}_n^*$ defines as:

$$\mathbf{m}_n^* = \begin{bmatrix} m_0^* \\ m_1^* \\ \vdots \\ m_n^* \end{bmatrix}, \quad m_k^* = \sum_{i=1}^{P} w_i \xi_i^k,$$

refer to the reconstructed moments of the approximation. A brief mechanism of the various EQMOM moment-inversion procedures proposed by (a) Yuan et al. [13], (b) Nguyen et al. [15] and (c) Pigou et al. [16] is summarized below:

(a) $A_{2P-1}^{-1}(\sigma)\begin{bmatrix} m_0 \\ \vdots \\ m_{2P-1} \end{bmatrix} = \begin{bmatrix} m_0^*(\sigma) \\ \vdots \\ m_{2P-1}^*(\sigma) \end{bmatrix}$

Calculate $\mathbf{a}_{P-1}^*(\sigma) = [a_0^*(\sigma), a_1^*(\sigma), \dots, a_{P-1}^*(\sigma)]^T$ and $\mathbf{b}_{P-1}^*(\sigma) = [b_1^*(\sigma), b_2^*(\sigma), \dots, b_{P-1}^*(\sigma)]^T$ recurring coefficients [21].

Find $\xi_P(\sigma)$ and $W_P(\sigma)$ vectors by calculating the eigenvalues and eigenvectors of the Jacobi matrix $J_{P-1}(d\mu)$ formed with the recurring coefficients.

$\hat{m}_{2P}(\sigma) = \sum_{i=1}^{P} w_i^*(\sigma)(\xi_i^*)^{2P}(\sigma)$

$\tilde{m}_{2P}(\sigma) = A_{2P}(\sigma)\begin{bmatrix} m_0^*(\sigma) \\ \vdots \\ m_{2P-1}^*(\sigma) \\ \hat{m}_{2P}(\sigma) \end{bmatrix}$, (see (16))

$D_{2P}(\sigma) = m_{2P} - \tilde{m}_{2P}(\sigma)$

(b) $A_{2P}^{-1}(\sigma)\begin{bmatrix} m_0 \\ \vdots \\ m_{2P-1} \end{bmatrix} = \begin{bmatrix} m_0^*(\sigma) \\ \vdots \\ m_{2P-1}^*(\sigma) \\ m_{2P}^*(\sigma) \end{bmatrix}$

Calculate $\mathbf{a}_{P-1}^*(\sigma) = [a_0^*(\sigma), a_1^*(\sigma), \dots, a_{P-1}^*(\sigma)]^T$ and $\mathbf{b}_{P-1}^*(\sigma) = [b_1^*(\sigma), b_2^*(\sigma), \dots, b_{P-1}^*(\sigma)]^T$ recurring coefficients.

Find $\xi_P(\sigma)$ and $W_P(\sigma)$ vectors by calculating the eigenvalues and eigenvectors of the Jacobi matrix $J_{P-1}(d\mu)$ formed with the recurring coefficients.

$\hat{m}_{2P}(\sigma) = \sum_{i=1}^{P} w_i^*(\sigma)(\xi_i^*)^{2P}(\sigma)$

$D_{2P}^*(\sigma) = m_{2P}^*(\sigma) - \tilde{m}_{2P}(\sigma)$

(c) $A_{2P}^{-1}(\sigma)\begin{bmatrix} m_0 \\ \vdots \\ m_{2P-1} \end{bmatrix} = \begin{bmatrix} m_0^*(\sigma) \\ \vdots \\ m_{2P-1}^*(\sigma) \\ m_{2P}^*(\sigma) \end{bmatrix}$

Calculate $\mathbf{a}_{P-1}^*(\sigma) = [a_0^*(\sigma), a_1^*(\sigma), \dots, a_{P-1}^*(\sigma)]^T$ and $\mathbf{b}_P^*(\sigma) = [b_1^*(\sigma), b_2^*(\sigma), \dots, b_P^*(\sigma)]^T$ recurring coefficients ($\Omega_\xi = \mathbb{R}$, the Hamburger problem).

The Stieljes problem: If $\Omega_\xi = (0, +\infty)$, the realisability of a moment set $\mathbf{m}_N^* = [m_0^*(\sigma), \dots, m_{2P-1}^*(\sigma), m_{2P}^*(\sigma)]$ on $\Omega_\xi = (0, \infty)$ is strictly equivalent to the positivity of the Hankel determinants H_{2P+d} defined as

$$H_{2P+d} = \begin{vmatrix} m_d^*(\sigma) & \dots & m_{P+d}^*(\sigma) \\ \vdots & \ddots & \vdots \\ m_{P+d}^*(\sigma) & \dots & m_{2P+d}^*(\sigma) \end{vmatrix} \tag{17}$$

with $d \in \{0,1\}$ and $P \in \mathbb{N}$, $2P + d \leq N$.
The condition for the positivity of Hankel determinants (17) can be written in terms of the positivity of ζ_k defined by

$$\zeta_k^*(\sigma) = \frac{H_{k-3}H_k}{H_{k-2}H_{k-1}}, \quad H_j = 1 \quad if \quad j < 0. \tag{18}$$

By using Eq.(18), the three-term recurring coefficients of the monic polynomials a_k^* and b_k^* coefficients can be written

$$b_k^*(\sigma) = \zeta_{2k}^*(\sigma)\zeta_{2k-1}^*(\sigma), \quad a_k^*(\sigma) = \zeta_{2k+1}^*(\sigma) + \zeta_{2k}^*(\sigma) \tag{19}$$

with $a_0^*(\sigma) = \zeta_1^*(\sigma)$ and the Jacobi matrix can be calculated. The recurring coefficients are calculated using Hankel determinants. Once the recurring coefficients a_n^* and b_n^* are known, the zeros of the orthogonal functions can be easily computed from the eigenvalues and eigenvectors of the Jacobi matrix. However, the ill-conditionality of Hankel matrices makes the formulas (19) not practically useful as an algorithm for calculating these coefficients. In particular, the function that computes the recurring coefficients from moments by using Eq.(19) and Eq.18 can be severely ill-conditioned [32,30] which means that the coefficients a_n^* and b_n^* are extremely sensitive to small changes in the moments.

The Hausdorff problem: If $\Omega_\xi = (0,1)$, compute
$\tau_{2P}^*(\sigma) = [\tau_0^*(\sigma), \tau_1^*(\sigma), \ldots, \tau_{2P}^*(\sigma)]^T$. Here, τ_{2P}^* vector elements can calculated from through the relation [33]

$$\tau_k^*(\sigma) = \frac{\zeta_k^*(\sigma)}{1 - \tau_{k-1}^*(\sigma)}$$

with $\zeta_k^*(\sigma)$ defined in Eq.(19) and $\tau_1^*(\sigma) = m_1^*(\sigma)$.

Here, the shape parameter σ is determined by enforcing an additional transported moment m_{2P} to accord with the reconstructed NDF. So, in (a) and (b), the roots of the $D_{2P}(\sigma)$ and $D_{2P}^*(\sigma)$ objective functions, if any, must be calculated, if not, their minimum values must be found. Due to the nonlinear dependence of $D_{2P}(\sigma)$ and D_{2P}^* on σ, it is inconvenient to find analytical expressions for the derivative $D_{2P}'(\sigma)$ and $(D_{2P}^*)'$. Thus to update σ, both the Ridder's method and a bounded secant method have been employed. If the Ridder's method can not find a root, the golden-section search method [14] is used to minimize the objective function. In (c) depending on Ω_ξ, the σ root, which is used for reconstructing NDF, is calculated with the help of sign change of $\mathbf{b}_{P-1}^*(\sigma)$, $\zeta_{2P}^*(\sigma)$ or $\tau_{2P}^*(\sigma)$ vectors and by updating σ values with the Ridder's method and using $[0, \sigma_1]$, where σ_1 is the analytical solution of $b_1^*(\sigma)$, $\zeta_2^*(\sigma)$ or $\tau_2^*(\sigma)$ depending on Ω_ξ. The above-mentioned procedures respond positively if there is one or more σ roots and at least one of the root falls within the given initial interval. In addition, if no σ falls within the initial interval or if there is no root, the optimum σ is calculated by golden-section search method which makes minimization in the initial interval.

4.2. Proposed moment-inversion procedure

While calculating the root of a function with iterative root-finding methods, the false position approach i.e. the search for the change of a function sign is typically used. However, when the difference between the roots of a function is small, it is difficult to approach this narrow range in which the function changes sign while searching the root of a function with only one root-finding algorithm. The Halley's approach point is thus calculated using the Ridder's approach point thereby improving the overall moment-inversion procedure.
In this section, while developing the moment-inversion procedure based on Halley-Ridder (H-R) method, the following cases have been examined in detail by assessing the evolution of convergence criteria:

1. a root falls within the given initial interval (shown with Hamburger, Stieltjes and Hausdorff moment problems).
2. multiple or very close roots fall within the given initial interval (shown with Hausdorff moment problem).
3. none of the roots fall within the given initial interval (shown with Hausdorff moment problem).
4. no root (shown with Stieltjes and Hausdorff moment problems).

Among these cases, for (3) and (4) the moment-inversion procedures mentioned in Section 4.1 do not respond. For (2), the procedures do not respond in finding the smallest root. The aim of this study, therefore, is to propose a method that will respond to all the cases (1-4). In the following section, the situations encountered for Hamburger, Stieltjes and Hausdorff problems using the proposed moment-inversion procedure are shown in detail.
There are essentially three different types of finite intervals: two end-points, one endpoint and no end-points [34]. In the latter case, the interval is $\mathbb{R}$ while in the first two cases they are (0, 1) and $[0, \infty)$ respectively. The moment problems on (0, 1), $[0, \infty)$ and $(-\infty, +\infty)$ are called the Hausdorff moment problem, the Stieltjes moment problem, and the Hamburger moment problem.

4.3. Hamburger moment problem

A necessary and sufficient condition that should exist is at least one non-decreasing function $d\mu(\xi) = \eta(\xi)d\xi$ such that

$$\mu_k = \int_{-\infty}^{\infty} \xi^k d\mu(\xi)$$

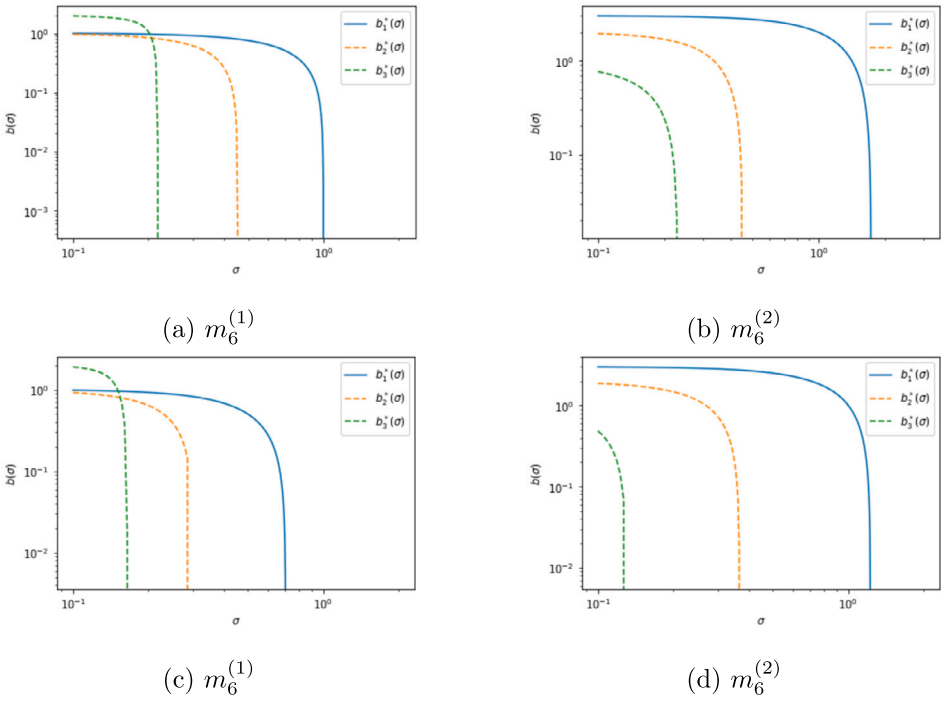

Fig. 1. Evolution of $b_k^*(\sigma)$ where $k = 1, 2, 3$, for Gaussian (a, b) and Laplace (c, d) kernels. The three initial moment sets are $m_6^{(1)} = [1 \quad 1 \quad 2 \quad 5 \quad 14 \quad 42 \quad 133]^T$ and $m_6^{(2)} = [1 \quad 2 \quad 7 \quad 17 \quad 58 \quad 149 \quad 493]^T$ as given in Pigou et al. [16].

for $k = 0, 1, 2, \ldots$, with all the integrals converging, the sequence $\{\mu_k\}_0^\infty$ is a positive definite [34].

4.3.1. Application of Halley-Ridder (H-R) method to the Hamburger problem

As stated in case (c) from Section 4.1, the metric $d\mu(\xi) = \eta(\xi)d\xi$ is realisable on $\Omega_\xi = (-\infty, +\infty)$ if and only if $a_k \in \mathbb{R}$ and $b_k > 0$, $\forall k \in \mathbb{N}$. A value of σ is searched such that the associated reconstructed moments $m_{2P-1}^*(\sigma)$ are strictly realisable, and the moments $m_{2P}^*(\sigma)$ are weakly realisable. Then if $\mathbf{a}_{P-1}^*(\sigma) = [a_0^*(\sigma), a_1^*(\sigma), \ldots, a_{P-1}^*(\sigma)]^T$ and $\mathbf{b}_{P-1}^*(\sigma) = [b_1^*(\sigma), b_2^*(\sigma), \ldots, b_{P-1}^*(\sigma)]^T$ recurring coefficients are calculated by the Chebyshev algorithm, the condition of realisability can be given by $\mathbf{b}_P^*(\sigma)$ as $b_k^*(\sigma) > 0$, $\forall k \in 1, 2, \ldots, P-1$ and $b_P^*(\sigma) = 0$. The evolution of $b_k^*(\sigma)$ $(k = 1, 2, 3)$ is shown in Fig. 1 for the Gaussian and Laplace kernels. The initial moments sets, $m_6^{(1)}$ and $m_6^{(2)}$ are taken from literature [16]. Several randomly selected moment sets are taken for testing purpose and an undefined root was never observed. According to these moment sets, the root σ_k being the root of $b_k(\sigma)$ lies within the interval $[0, \sigma_{k-1}]$. It must be noted here that a mathematical proof of these observations has not been provided by Pigou et al. [16]. Therefore, there is a possibility that the root σ_k, being the root of $b_k^*(\sigma)$, can be outside the interval $[0, \sigma_{k-1}]$. Considering this possibility, a more robust procedure is needed. It can be given as an iterative approach as follows:

1. $[0, 1] = [\sigma_l^{(0)}, \sigma_r^{(0)}]$ is the initial interval, then update these bounds.
2. Compute $\mathbf{b}_P(0)$; check the realisability of $m_{2P} = m_{2P}^*$ and check the positivity of the elements in the vector $\mathbf{b}_P(0)$.
3. Iterate over k
   - Compute $\mathbf{b}_P(\sigma_r^{(k-1)})$ and check if $\mathbf{b}_P(\sigma_r^{(k-1)})$ has at least one negative element.
   - if $\mathbf{b}_P(\sigma_r^{(k-1)})$ has at least one negative element.
     - (a) Choose σ_t.
     - (b) Compute $\mathbf{b}_P(\sigma_t)$
     - (c) if all elements of $\mathbf{b}_P(\sigma_t)$ are positive, assign $\sigma_l^l = \sigma_t$ and $\sigma_r^{(k)} = \sigma_r^{(k-1)}$.
     - (d) otherwise, assign $\sigma_l^l = \sigma_r^{(k-1)}$ and $\sigma_r^{(k)} = \sigma_t$.
   - if all elements of $\mathbf{b}_P(\sigma_r^{(k-1)})$ are positive
     - (a1) Choose σ_t
     - (b1) Compute $\mathbf{b}_P(\sigma_t)$ and check if $\mathbf{b}_P(\sigma_t)$ has at least one negative element.
     - (c1) if $\mathbf{b}_P(\sigma_t)$ has at least one negative element, apply (a), (b), (c) and (d) steps
     - else
       * if $b_P^*(\sigma_t) < b_P^*(\sigma_r^{(k-1)})$, assign $\sigma_r^{(k)} = \sigma_t$.
       * if $b_P^*(\sigma_l^{(k-1)}) > b_P^*(\sigma_t)$, assign $\sigma_r^{(l)} = \sigma_t$

In Pigou et al. [16], the choice of σ_t in steps 3(a) and 3(a1) are made by locating the root σ_j of $b_j^*(\sigma)$ with j as the index of the first negative element of $\mathbf{b}_P^*(\sigma_r^{(k)})$. σ_t is selected by using Ridder's method [14], which tests two σ values per iteration. At this stage, Halley-Ridder (H-R) method is proposed which tests three σ values per iteration for step 3(a), and makes minimization by using a hybridization approach to move out of the initial interval. The procedure is given as follows:

- Compute $\mathbf{b}_P(0)$; check the realisability of $m_{2P} = m_{2P}^*$ and check the positivity of the elements in the vector $\mathbf{b}_P(0)$.
- $[\sigma_l^{(0)}, \sigma_r^{(0)}] = [0, 1]$ (initial interval)
- Iterate over k
  - Identify j, if defined
    - $\sigma_{t_1} = \dfrac{\sigma_l^{(k-1)} - \sigma_r^{(k-1)}}{2}$
    - $\sigma_{t_2} = \sigma_{t_1} + (\sigma_{t_1} - \sigma_l^{(k-1)}) \dfrac{b_j^*(\sigma_{t_1})}{\sqrt{b_j^*(\sigma_{t_1})^2 - b_j^*(\sigma_l^{(k-1)}) * b_j^*(\sigma_r^{(k-1)})}}$
    - $X = \dfrac{b_j^*(\sigma_r^{(k-1)}) - b_j^*(\sigma_{t_2})}{\sigma_r^{(k-1)} - \sigma_{t_2}}$
    - $Y = \dfrac{b_j^*(\sigma_{t_2}) - b_j^*(\sigma_l^{(k-1)})}{\sigma_{t_2} - \sigma_l^{(k-1)}}$
    - $Z = \dfrac{X - Y}{\sigma_r^{(k-1)} - \sigma_l^{(k-1)}}$
    - $\sigma_{t_3} = \sigma_r^{(k-1)} - \dfrac{2b_j^*(\sigma_r^{(k-1)})X}{2X^2 - b_j^*(\sigma_r^{(k-1)})Z}$
    - Set $\sigma_l^{(k)}$ as the maximum value among $\sigma_l^{(k-1)}$, σ_{t_1}, σ_{t_2} and σ_{t_3} such that all elements of the vector $\mathbf{b}_P^*$ are positive.
    - Set $\sigma_r^{(k)}$ as the minimum value among $\sigma_r^{(k-1)}$, σ_{t_1}, σ_{t_2} and σ_{t_3} such that at least one element of the vector $\mathbf{b}_P^*$ is negative.
  - else
    - $\sigma_{t_1} = \dfrac{\sigma_l^{(k-1)} - \sigma_r^{(k-1)}}{2}$
    - $\sigma_{t_2} = \sigma_r^{(k-1)} + \sigma_{t_1} + (\sigma_{t_1} - \sigma_l^{(k-1)}) \dfrac{b_P^*(\sigma_{t_1})}{\sqrt{\mid b_P^*(\sigma_{t_1})^2 - b_P^*(\sigma_l^{(k-1)}) * b_P^*(\sigma_r^{(k-1)}) \mid}}$
    - $X = \dfrac{b_P^*(\sigma_r^{(k-1)}) - b_P^*(\sigma_{t_2})}{\sigma_r^{(k-1)} - \sigma_{t_2}}$
    - $Y = \dfrac{b_P^*(\sigma_{t_2}) - b_P^*(\sigma_l^{(k-1)})}{\sigma_{t_2} - \sigma_l^{(k-1)}}$
    - $Z = \dfrac{X - Y}{\sigma_r^{(k-1)} - \sigma_l^{(k-1)}}$
    - $\sigma_{t_3} = \mid 2\sigma_r^{(k-1)} - \dfrac{2b_P^*(\sigma_r^{(k-1)})X}{2X^2 - b_P^*(\sigma_r^{(k-1)})Z} \mid$
    - Identify j
    - if the negative element defined for both $\mathbf{b}_P^*(\sigma_{t_2}^{(k-1)})$ and $\mathbf{b}_P^*(\sigma_{t_3}^{(k-1)})$, assign $\sigma_l^{k+1} = \sigma_r^{(k-1)}$. If $\sigma_{t_2}^{(k-1)} > \sigma_{t_3}^{(k-1)}$ then assign $\sigma_r^{(k+1)} = \sigma_{t_3}^{(k-1)}$ else $\sigma_r^{(k+1)} = \sigma_{t_2}^{(k-1)}$.
    - Only if the negative element of $\mathbf{b}_P^*(\sigma_{t_2}^{(k-1)})$, assign $\sigma_l^{k+1} = \sigma_r^{(k-1)}$ and $\sigma_r^{(k+1)} = \sigma_{t_2}^{(k-1)}$.
    - Only if the negative element of $\mathbf{b}_P^*(\sigma_{t_3}^{(k-1)})$, assign $\sigma_l^{k+1} = \sigma_r^{(k-1)}$ and $\sigma_r^{(k+1)} = \sigma_{t_3}^{(k-1)}$.
    - if no j is defined
      - Calculate $b_P^*(\sigma_l^{(k-1)})$, $b_P^*(\sigma_r^{(k-1)})$, $b_P^*(\sigma_{t_1})$, $b_P^*(\sigma_{t_2})$ and $b_P^*(\sigma_{t_3})$.
      - Assign those $\sigma_l^{(k-1)}$, $\sigma_r^{(k-1)}$, σ_{t_1}, σ_{t_2} and σ_{t_3} that correspond to the two smallest b_P^* values in absolute value as $\sigma_l^{(k-1)}$ and $\sigma_r^{(k-1)}$.

For simplicity, $[0, 1]$ is taken as the initial interval. The computation is stopped if $\sigma_r^{(k)} - \sigma_l^{(k)} < \epsilon$ or $b_P^*(\sigma_l^k) < \epsilon b_P^*(0)$, with ϵ as a relative tolerance. Then the weights w_P and nodes ξ_P of the reconstruction are computed using a Gauss quadrature based on recurring coefficients $\mathbf{a}^*(\sigma_l^{(k)})$ and $\mathbf{b}^*(\sigma_l^{(k)})$.

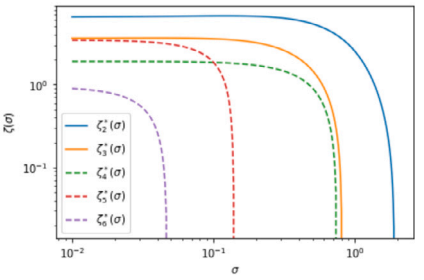

(a) $m_6^{(a)}$

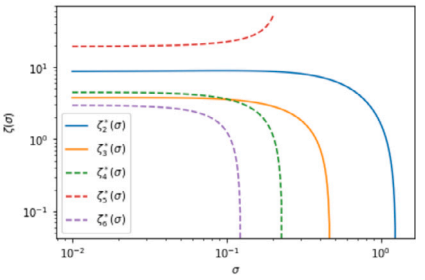

(b) $m_6^{(b)}$

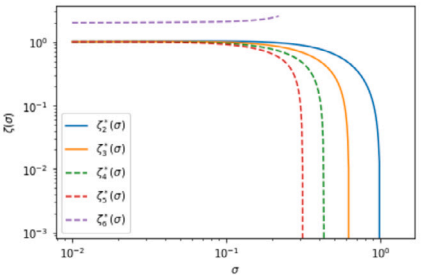

(c) $m_6^{(c)}$

Fig. 2. Evolution of $\zeta_k^*(\sigma)$, where $k = 2,3,4,5,6$ for Weibull kernel. The initial moment sets are $m_6^{(a)} = [1 \quad 1.5 \quad 12 \quad 131 \quad 1520 \quad 18033 \quad 2.16e5]^T$, $m_6^{(b)} = [1 \quad 5.5 \quad 78 \quad 1285 \quad 22225 \quad 4.05e5 \quad 7.88e6]^T$ and $m_6^{(c)} = [1 \quad 1 \quad 2 \quad 5 \quad 14 \quad 42 \quad 133]^T$ as given in Pigou et al. [16].

4.4. Stieltjes moment problem

A necessary and sufficient condition that there should exist at least one non-decreasing function $d\mu(\xi) = \eta(\xi)d\xi$ such that

$$\mu_k = \int_0^\infty \xi^k d\mu(\xi)$$

for $k = 0, 1, 2, \ldots$, with all the integrals converging, is that the sequence $\{\mu_k\}_0^\infty$ is positive definite [34].

4.4.1. Application of Halley-Ridder (H-R) method to the Stieltjes problem

As stated in case (c) from Section 4.1, one of the realisability criteria to calculate the parameters of the quadrature is looking for σ such that $\zeta_k^*(\sigma) > 0$, $\forall k \in 1, 2, \ldots, N-1$ and $\zeta_N^*(\sigma) = 0$. Several randomly selected moment sets are taken for testing purpose. Fig. 2 shows the evolution of $\zeta_k^*(\sigma)$, $k = 2,3,4,5,6$ for three moment sets taken from Pigou et al. [16] when used for the Weibull kernel. Fig. 2a shows all the roots σ_k, $k \in 2, 3, \ldots, N$ are defined, Fig. 2b shows the root σ_N exist while some roots σ_k, $k \in 3, 4, \ldots, N-1$, are not defined and Fig. 2c shows the root σ_N is not defined.

In the first and second situations, the EQMOM approximation is well defined, because σ_N exists. In the third situation, the root σ_N does not exist in the range, where $\zeta_k^*(\sigma)$, $k \in 2, 3, \ldots, N-1$ are positive. So instead of root finding algorithm, minimization is required here.

Similarly, the method for reconstruction of kernels defined in $\Omega_\xi = (0, +\infty)$ can be given in Section 4.3.1 by making a little adjustment:

- Compute $\zeta_N^*(0)$; check the realisability of $m_{2P} = m_{2P}^*$ and check the positivity of the elements in the vector $\zeta_N^*(0)$.
- $[\sigma_l^{(0)}, \sigma_r^{(0)}] = [0, 1]$ (initial interval)
- Iterate over k
  - Identify j, if defined
    - $\sigma_{t_1} = \dfrac{\sigma_l^{(k-1)} - \sigma_r^{(k-1)}}{2}$
    - $\sigma_{t_2} = \sigma_{t_1} + (\sigma_{t_1} - \sigma_l^{(k-1)}) \dfrac{\zeta_j^*(\sigma_{t_1})}{\sqrt{\zeta_j^*(\sigma_{t_1})^2 - \zeta_j^*(\sigma_l^{(k-1)}) * \zeta_j^*(\sigma_r^{(k-1)})}}$
    - $X = \dfrac{\zeta_j^*(\sigma_r^{(k-1)}) - \zeta_j^*(\sigma_{t_2})}{\sigma_r^{(k-1)} - \sigma_{t_2}}$

* $Y = \dfrac{\zeta_j^*(\sigma_{t_2}) - \zeta_j^*(\sigma_l^{(k-1)})}{\sigma_{t_2} - \sigma_l^{(k-1)}}$
* $Z = \dfrac{X - Y}{\sigma_r^{(k-1)} - \sigma_l^{(k-1)}}$
* $\sigma_{t_3} = \sigma_r^{(k-1)} - \dfrac{2\zeta_j^*(\sigma_r^{k-1})X}{2X^2 - \zeta_j^*(\sigma_r^{(k-1)})Z}$
* Set $\sigma_l^{(k)}$ as the maximum value among $\sigma_l^{(k-1)}$, σ_{t_1}, σ_{t_2} and σ_{t_3} such that all the elements of the vector ζ_N^* are positive.
* Set $\sigma_r^{(k)}$ as the minimum value among $\sigma_r^{(k-1)}$, σ_{t_1}, σ_{t_2} and σ_{t_3} such that at least one of element of the vector ζ_N^* is negative.

– else

* $\sigma_{t_1} = \dfrac{\sigma_l^{(k-1)} - \sigma_r^{(k-1)}}{2}$
* $\sigma_{t_2} = \sigma_r^{(k-1)} + \sigma_{t_1} + (\sigma_{t_1} - \sigma_l^{(k-1)}) \dfrac{\zeta_{2P}^*(\sigma_{t_1})}{\sqrt{|\,\zeta_{2P}^*(\sigma_{t_1})^2 - \zeta_{2P}^*(\sigma_l^{(k-1)}) * \zeta_{2P}^*(\sigma_r^{(k-1)})\,|}}$
* $X = \dfrac{\zeta_{2P}^*(\sigma_r^{(k-1)}) - \zeta_{2P}^*(\sigma_{t_2})}{\sigma_r^{(k-1)} - \sigma_{t_2}}$
* $Y = \dfrac{\zeta_{2P}^*(\sigma_{t_2}) - \zeta_{2P}^*(\sigma_l^{(k-1)})}{\sigma_{t_2} - \sigma_l^{(k-1)}}$
* $Z = \dfrac{X - Y}{\sigma_r^{(k-1)} - \sigma_l^{(k-1)}}$
* $\sigma_{t_3} = |\, 2\sigma_r^{(k-1)} - \dfrac{2\zeta_{2P}^*(\sigma_r^{(k-1)})X}{2X^2 - \zeta_{2P}^*(\sigma_r^{(k-1)})Z}\,|$
* Identify j.
* if the negative element is defined for both $\zeta_N^*(\sigma_{t_2}^{(k-1)})$ and $\zeta_N^*(\sigma_{t_3}^{(k-1)})$, assign $\sigma_l^{k+1} = \sigma_r^{(k-1)}$. If $\sigma_{t_2}^{(k-1)} > \sigma_{t_3}^{(k-1)}$ then assign $\sigma_r^{(k+1)} = \sigma_{t_3}^{(k-1)}$ else $\sigma_r^{(k+1)} = \sigma_{t_2}^{(k-1)}$.
* Only if the negative element of $\zeta_N^*(\sigma_{t_2}^{(k-1)})$ exists, assign $\sigma_l^{k+1} = \sigma_r^{(k-1)}$ and $\sigma_r^{(k+1)} = \sigma_{t_2}^{(k-1)}$.
* Only if the negative element of $\zeta_N^*(\sigma_{t_3}^{(k-1)})$ exists, assign $\sigma_l^{k+1} = \sigma_r^{(k-1)}$ and $\sigma_r^{(k+1)} = \sigma_{t_3}^{(k-1)}$.
* if no j is defined
  · Calculate $\zeta_{2P}^*(\sigma_l^{(k-1)})$, $\zeta_{2P}^*(\sigma_r^{(k-1)})$, $\zeta_{2P}^*(\sigma_{t_1})$, $\zeta_{2P}^*(\sigma_{t_2})$ and $\zeta_{2P}^*(\sigma_{t_3})$.
  · Assign those $\sigma_l^{(k-1)}$, $\sigma_r^{(k-1)}$, σ_{t_1}, σ_{t_2} and σ_{t_3} that correspond to the two smallest b_P^* values in absolute value as $\sigma_l^{(k-1)}$ and $\sigma_r^{(k-1)}$.

Stop the computation if $\sigma_r^{(k)} - \sigma_l^{(k)} < \epsilon$ or $\zeta_N^*(\sigma_l^k) < \epsilon\zeta_N^*(0)$, with ϵ as a relative tolerance. Then the weights w_P and nodes ξ_P of the reconstruction are computed using a Gauss quadrature based on recurring coefficients $\mathbf{a}^*(\sigma_l^{(k)})$ and $\mathbf{b}^*(\sigma_l^{(k)})$.

4.5. Hausdorff moment problem

A sufficient and necessary condition is that there should exist at least one non-decreasing function $d\mu(\xi) = \eta(\xi)d\xi$ such that

$$\mu_k = \int_0^1 \xi^k \, d\mu(\xi)$$

for $k = 0, 1, 2, \ldots$, with all the integrals converging the sequence $\{\mu_k\}_0^\infty$ is a positive definite [34].

4.5.1. Application of Halley-Ridder (H-R) method to the Hausdorff problem

As stated in case (c) from Section 4.1, one of the realisability criteria of EQMOM moment-inversion procedure is to compute for σ such that $\tau_k^*(\sigma) \in (0, 1)$, $\forall k \in 1, 2, \ldots, N-1$ and $\tau_N^*(\sigma) = 0$. Several randomly selected moment sets are taken for testing purpose. For the Beta kernel, the evolution of $\tau_k^*(\sigma)$, $k = 2, 3, 4, 5, 6$ is shown in Fig. 3 such that the initial moment sets are

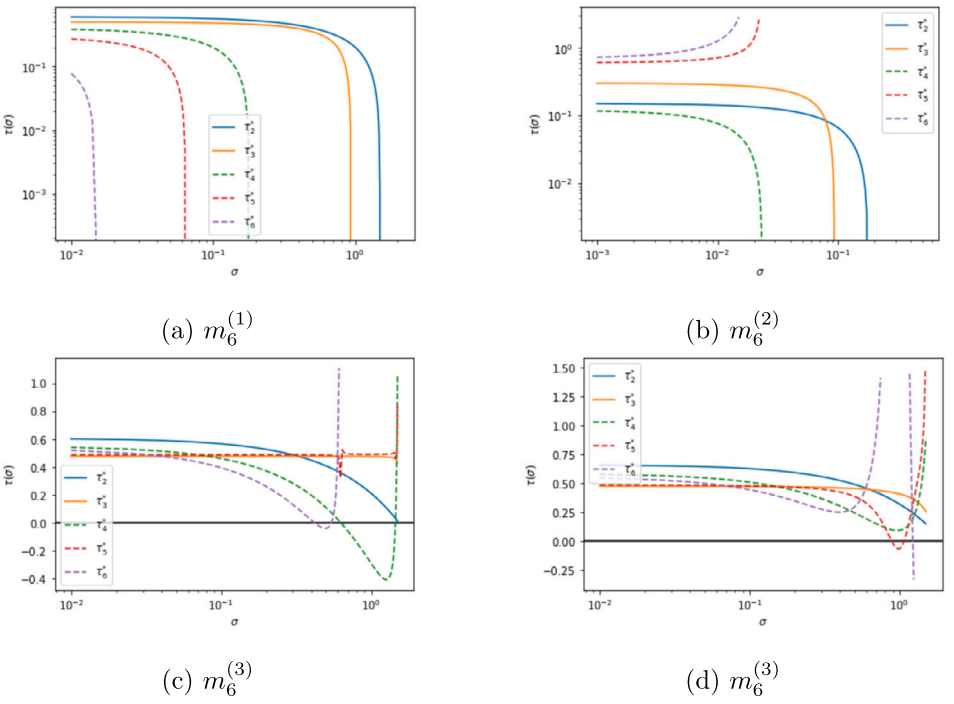

Fig. 3. Evolution of $\tau_k^*(\sigma)$, where $k = 2, 3, 5, 6$ for Beta kernel with the initial moments sets mentioned in Eq. (20).

$$
m_6^{(1)} = \begin{bmatrix} 1 \\ 0.8 \\ 0.736 \\ 0.69632 \\ 0.6659584 \\ 0.640222208 \\ 0.61713719296 \end{bmatrix}
m_6^{(2)} = \begin{bmatrix} 1 \\ 0.5 \\ 0.2875 \\ 0.174875 \\ 0.10929325 \\ 0.0695751215 \\ 0.045108235453 \end{bmatrix}
$$

$$
m_6^{(3)} = \begin{bmatrix} 1 \\ 0.409890129103329 \\ 0.314508552447814 \\ 0.268912990299659 \\ 0.240626997247657 \\ 0.220778450679946 \\ 0.205805473717484 \end{bmatrix},
m_6^{(4)} = \begin{bmatrix} 1 \\ 0.445967016759259 \\ 0.361907331989521 \\ 0.320071825637556 \\ 0.293507585949640 \\ 0.274561571617238 \\ 0.260088628766843 \end{bmatrix}
\tag{20}
$$

which are taken from Pigou et al. [16]. The explanation of Figs. 3(a-d) are as follows:

- Fig. 3a: the root σ_N of $\tau_{2P}^*(\sigma)$ exists and the EQMOM Beta kernel is well defined
- Fig. 3b: the root σ_N and σ_{N-1} are not defined in the interval, where $\tau_k^*(\sigma)$, $k \in 2, 3, \ldots, N-2$ are all positive.
- Fig. 3c: $\tau_N^*(\sigma)$ has more than a root.
- Fig. 3d: σ_N is defined but there is an interval in which convergence criteria is undefined.

The procedure given in Section 4.3.1 can be applied to the Hausdorff problem by checking if all of the elements of $\tau_{2P}^*(\sigma)$ fall into the interval $(0, 1)$.

- Check the realisability of $\mathbf{m}_{2P} = \mathbf{m}_{2P}^*$ by computing $\tau_N^*(0)$ and check if all elements fall into $(0, 1)$
- $[\sigma_l^{(0)}, \sigma_r^{(0)}] = [0, 1]$ (initial interval) and σ_2 is the analytic solution of $\tau_2^*(\sigma)$
- Iterate over k
  - identify j as the index of the first element of $\tau_N^*(\sigma_r^{(k-1)})$ being negative or higher than 1, if defined
    - $\sigma_{t_1} = \dfrac{\sigma_l^{(k-1)} - \sigma_r^{(k-1)}}{2}$
    - if $j < N$ and $\tau_j^*(\sigma_r^{(k-1)}) > 1$,

· $\sigma_{t_2} = \sigma_{t_1} + (\sigma_{t_1} - \sigma_l^{(k-1)}) \dfrac{1 - \tau_j^*(\sigma_{t_1})}{\sqrt{(1 - \tau_j^*(\sigma_{t_1}))^2 - (1 - \tau_j^*(\sigma_l^{(k-1)})) * (1 - \tau_j^*(\sigma_r^{(k-1)}))}}$

* if $j = N$ or $\tau_j^*(\sigma_r^{(k-1)}) < 0$

· $\sigma_{t_2} = \sigma_{t_1} + (\sigma_{t_1} - \sigma_l^{(k-1)}) \dfrac{\tau_j^*(\sigma_{t_1})}{\sqrt{\tau_j^*(\sigma_{t_1})^2 - \tau_j^*(\sigma_l^{(k-1)}) * \tau_j^*(\sigma_r^{(k-1)})}}$

* $X = \dfrac{\tau_j^*(\sigma_r^{(k-1)}) - \tau_j^*(\sigma_{t_2})}{\sigma_r^{(k-1)} - \sigma_{t_2}}$

* $Y = \dfrac{\tau_j^*(\sigma_{t_2}) - \tau_j^*(\sigma_l^{(k-1)})}{\sigma_{t_2} - \sigma_l^{(k-1)}}$

* $Z = \dfrac{X - Y}{\sigma_r^{(k-1)} - \sigma_l^{(k-1)}}$

* if $j = N$ or $\tau_j^*(\sigma_r^{(k-1)}) < 0$

· $\sigma_{t_3} = \sigma_r^{(k-1)} - \dfrac{2(1 - \tau_j^*(\sigma_r^{k-1}))Z}{2Z^2 - (1 - \tau_j^*(\sigma_r^{(k-1)}))Z}$

* if $j = N$ or $\tau_j^*(\sigma_r^{(k-1)}) < 0$

· $\sigma_{t_3} = \sigma_r^{(k-1)} - \dfrac{2\tau_j^*(\sigma_r^{k-1})Z}{2Z^2 - \tau_j^*(\sigma_r^{(k-1)})Z}$

– else

* $\sigma_{t_1} = \dfrac{\sigma_l^{(k-1)} - \sigma_r^{(k-1)}}{2}$

* $\sigma_{t_2} = \sigma_r^{(k-1)} + \sigma_{t_1} + (\sigma_{t_1} - \sigma_l^{(k-1)}) \dfrac{\tau_{2P}^*(\sigma_{t_1})}{\sqrt{|\, \tau_{2P}^*(\sigma_{t_1})^2 - \tau_{2P}^*(\sigma_l^{(k-1)}) * \tau_{2P}^*(\sigma_r^{(k-1)}) \,|}}$

* $X = \dfrac{\tau_{2P}^*(\sigma_r^{(k-1)}) - \tau_{2P}^*(\sigma_{t_2})}{\sigma_r^{(k-1)} - \sigma_{t_2}}$

* $Y = \dfrac{\tau_{2P}^*(\sigma_{t_2}) - \tau_{2P}^*(\sigma_l^{(k-1)})}{\sigma_{t_2} - \sigma_l^{(k-1)}}$

* $Z = \dfrac{X - Y}{\sigma_r^{(k-1)} - \sigma_l^{(k-1)}}$

* $\sigma_{t_3} = | \, 2\sigma_r^{(k-1)} - \dfrac{2\tau_{2P}^*(\sigma_r^{(k-1)})X}{2X^2 - \tau_{2P}^*(\sigma_r^{(k-1)})Z} \, |$

* Identify j as the index of the first negative or bigger than 1 element of $\tau_N^*(\sigma_{t_2}^{(k-1)})$ and $\tau_N^*(\sigma_{t_2}^{(k-1)})$.

* if the negative or bigger than 1 element defined for both $\tau_N^*(\sigma_{t_2}^{(k-1)})$ and $\zeta_N^*(\sigma_{t_3}^{(k-1)})$, assign $\sigma_l^{k+1} = \sigma_r^{(k-1)}$. If $\sigma_{t_2}^{(k-1)} > \sigma_{t_3}^{(k-1)}$ then assign $\sigma_r^{(k+1)} = \sigma_{t_3}^{(k-1)}$ else $\sigma_r^{(k+1)} = \sigma_{t_2}^{(k-1)}$.

* Only if the negative or bigger than 1 element of $\tau_N^*(\sigma_{t_2}^{(k-1)})$ is defined, assign $\sigma_l^{k+1} = \sigma_r^{(k-1)}$ and $\sigma_r^{(k+1)} = \sigma_{t_2}^{(k-1)}$.

* Only if the negative or bigger than 1 element of $\tau_N^*(\sigma_{t_3}^{(k-1)})$ is defined, assign $\sigma_l^{k+1} = \sigma_r^{(k-1)}$ and $\sigma_r^{(k+1)} = \sigma_{t_3}^{(k-1)}$.

* if no j is defined

· Calculate $\tau_{2P}^*(\sigma_l^{(k-1)})$, $\tau_{2P}^*(\sigma_r^{(k-1)})$, $\tau_{2P}^*(\sigma_{t_1})$, $\tau_{2P}^*(\sigma_{t_2})$ and $\tau_{2P}^*(\sigma_{t_3})$.

· Assign those $\sigma_l^{(k-1)}$, $\sigma_r^{(k-1)}$, σ_{t_1}, σ_{t_2} and σ_{t_3} that correspond to the two smallest b_P^* values in absolute value as $\sigma_l^{(k-1)}$ and $\sigma_r^{(k-1)}$.

– if $\tau_N^*(\sigma_l^k) > \epsilon\tau_N^*(0)$, update initial interval as $[1, \sigma_2]$ and run the procedure by making the if queries before else for $\sigma_l^{(k-1)}$.

Stop the computation if $\sigma_r^{(k)} - \sigma_l^{(k)} < \epsilon$ or $\tau_N^*(\sigma_l^k) < \epsilon\tau_N^*(0)$, with ϵ as a relative tolerance. For $\tau_N^*(\sigma_l^k) > \epsilon\tau_N^*(0)$, if the algorithm cannot find σ_P in the range $[1, \sigma_2]$, the σ_P found in the range $[0, 1]$ is used. Then the weights w_P and nodes ξ_P of the reconstruction are computed using a Gauss quadrature based on recurring coefficients $\mathbf{a}^*(\sigma_l^{(k)})$ and $\mathbf{b}^*(\sigma_l^{(k)})$.

5. Tested moment sets

A sufficient and necessary condition is that there should exist at least one non-decreasing function $d\mu(\xi) = \eta(\xi)d\xi$ such that The H-R method is tested for several kernels defined on: Gauss and Laplace kernels where $\Omega_\xi = (-\infty, \infty)$, Gamma and Weibull kernels where $\Omega_\xi = (0, +\infty)$ and Beta kernel where $\Omega_\xi = (0, 1)$, using Python implementations. Also, to see gain in number of tested σ values,

the procedure [16] is performed for the same kernels, using Python 3.10. The gain indicates the percentage by which the number of iterations decreases in the proposed Halley-Ridder's method as compared to Ridder's method used by Pigou et al. [16].

Since the moment-inversion procedure used in this study is obtained by improving the moment-inversion procedure of Pigou et al. [16], it is necessary to know how these tested moment sets are obtained. Moments sets for Log-normal, Gauss, and Laplace kernels defined on $\Omega_\xi = (-\infty, \infty)$ were both taken from [16] and were constructed by random vectors $\mathbf{a}_{P-1}$ and $\mathbf{b}_P$ using a reversed Chebyshev algorithm. The elements of these vectors are calculated by the following distribution laws:

$$a_k \sim \mathcal{N}(0, 25), \quad k \in 0, \ldots, P-1$$
$$b_k \sim 1 + Exp(4), \quad k \in 1, \ldots, P$$

Similarly, moments sets for Gamma and Weibull kernels defined on $\Omega_\xi = (0, +\infty)$ were both taken from [16] and constructed by random vectors ζ_{2P} using a reversed ζ-Chebyshev algorithm. The elements of these vectors are calculated using:

$$\zeta_k \sim 1 + Exp(4), \quad k \in 1, \ldots, 2P$$
$$\zeta_{2P} \sim Exp(0.5)$$

Also, moments sets for kernel defined on $\Omega_\xi = (0, 1)$ were constructed by random vectors τ_{2P} using a reversed τ-Chebyshev algorithm. Elements of these vectors are calculated using:

$$\tau_k \sim \mathcal{U}(0, 1), \quad k \in 1, \ldots, 2P.$$

Using the proposed Halley-Ridder moment-inversion procedure, the number of iterations required for the convergence is calculated for the tested moment sets.

6. Results and discussions

The H-R method proposed in this study and the method proposed by Pigou et al. [16] are applied to the moments sets obtained from [16]. Table 1 shows the results of these two methods which indicates a reduction in the number of σ values. Since the H-R method shows a decrease compared to the method used by Pigou et al. [16] in terms of tested σ values, it also means a decrease compared to the method used by Nguyen et al. [15]. This reduction is mainly due to the H-R methodology which gives a better choice for the tested shape parameter σ values and uses three values to update the interval while the method of Pigou et al. [16] used two values. The coefficient of variation in the number of σ values for each tested Kernel Density Functions (KDFs) is shown by the ratio of standard deviation to mean in Table 2. As seen in the table, there is no significant difference between the Halley-Ridder method used in this study and Ridder's method used in Pigou et al. [16]. In other words, there is no significant difference in the extent of variability of the two procedures relative to the mean of the tested σ values. In the proposed H-R method, because of using three values to update the range, an increase in the number of floating point operations (FLOPS) can be observed with a decrease in the number of σ values. The increase in number of FLOPS using the H-R method compared to the method proposed by Pigou et al. [16] is shown in Table 3 for all tested kernels and moment sets by considering linear system, Chebyshev algorithm and calculation of the root σ_P. From Table 1 and Table 3, it can be seen that as the number of σ values decreases, the difference in number of FLOPS between the two methods also decreases. Both conditions of moment sets being near the boundary and far from the boundary of the realisable moment space are tested. However, it did not have an effect on increasing or decreasing the σ values and FLOPS numbers. The most expensive operation in both the methods is the calculation of eigenvalues and eigenvectors of the tridiagonal symmetric matrix where the Jacobi algorithm was used. As a suggestion, divide and conquer algorithm [35] can be used instead of Jacobi algorithm because an advantage is that it can be used to calculate all or part of the eigenvalues of a symmetric matrix using parallel computation.

Moreover, for Beta kernel defined in $\Omega_\xi = (0, 1)$ in the case given in Fig. 3(c), the lowest root is calculated by the H-R method even they are very close to each other. So a small change in the raw moments will only cause a small change in the resulting shape

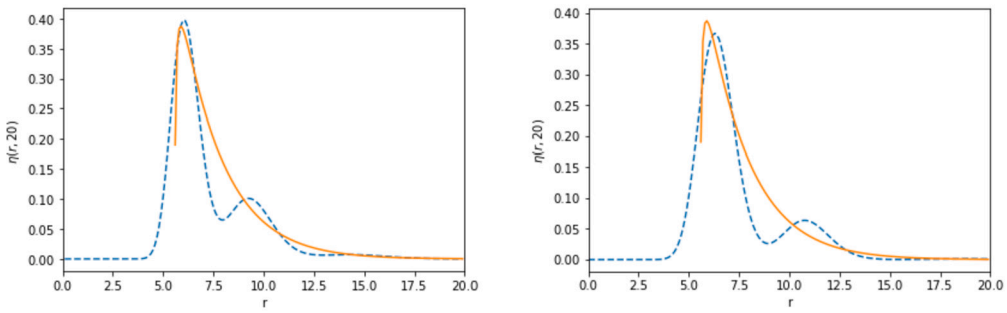

Fig. 4. Evolution of number density function (NDF) at $t = 20$ ($\eta(r, 20)$): exact (solid orange line) vs. numerical (dashed blue line) with LogN KDF (left) for $P = 3$ and Gamma KDF (right) for $P = 4$, for diffusion-controlled growth.

Table 1
Difference in gain for all the tested kernels and moment sets used in this study in comparison to Pigou et al. [16]. The numbers indicate a statistical average of 10,000 moment sets.

Tested kernels	Realisability of moment set	P = 2	P = 3	P = 4	P = 5
Gauss	Strict	$30.3_{\pm 9.4}$	$29.8_{\pm 5.1}$	$32.7_{\pm 8.7}$	$22.3_{\pm 4.8}$
	Weak	$19.8_{\pm 1.2}$	$17.8_{\pm 11.5}$	$16.8_{\pm 7.1}$	$17.0_{\pm 3.5}$
Laplace	Strict	$21.4_{\pm 23.0}$	$24.0_{\pm 6.8}$	$21.0_{\pm 11.8}$	$20.2_{\pm 8.0}$
	Weak	$10.2_{\pm 6.3}$	$35.4_{\pm 13.4}$	$15.0_{\pm 10.3}$	$15.4_{\pm 2.2}$
Log-normal	Strict	$37.3_{\pm 36.5}$	$25.0_{\pm 37.6}$	$16.6_{\pm 62.8}$	$10.3_{\pm 36.0}$
	Weak	$34.3_{\pm 58.6}$	$21.9_{\pm 40.5}$	$12.8_{\pm 25.5}$	$4.6_{\pm 20.2}$
Gamma	Strict	$33.1_{\pm 35.2}$	$33.6_{\pm 15.8}$	$32.2_{\pm 27.3}$	$28.0_{\pm 19.2}$
	Weak	$43.6_{\pm 71.3}$	$33.2_{\pm 36.8}$	$33.7_{\pm 28.5}$	$28.9_{\pm 21.8}$
Weibull	Strict	$33.9_{\pm 38.1}$	$20.8_{\pm 24.8}$	$14.7_{\pm 22.0}$	$13.5_{\pm 23.8}$
	Weak	$41.8_{\pm 58.8}$	$29.5_{\pm 32.5}$	$14.6_{\pm 11.7}$	$10.5_{\pm 4.6}$

Table 2
Coefficient of variation (standard deviation/mean) for the distribution of tested shape parameter σ values for various kernels. Only moment sets generated far from the realisable moment space are considered.

Tested kernels	Realisability of moment set	P = 2	P = 3	P = 4	P = 5
Gauss	this study	0.29	0.24	0.23	0.22
	Pigou et al. [16]	0.18	0.18	0.16	0.16
Laplace	this study	0.30	0.25	0.22	0.21
	Pigou et al. [16]	0.19	0.18	0.16	0.16
Log-normal	this study	0.25	0.19	0.17	0.16
	Pigou et al. [16]	0.25	0.23	0.23	0.23
Gamma	this study	0.38	0.27	0.20	0.21
	Pigou et al. [16]	0.39	0.21	0.19	0.18
Weibull	this study	0.26	0.21	0.19	0.18
	Pigou et al. [16]	0.27	0.22	0.21	0.21

Table 3
Difference in the number of FLOPS for all the tested kernels and moment sets used in this study in comparison to Pigou et al. [16]. The numbers indicate a statistical average of 10,000 moment sets.

Tested kernels	Realisability of moment set	P = 2	P = 3	P = 4	P = 5
Gauss	Strict	$30.9_{\pm 16.6}$	$25.3_{\pm 9.8}$	$21.1_{\pm 7.6}$	$23.0_{\pm 7.2}$
	Weak	$47.3_{\pm 19.9}$	$38.3_{\pm 15.3}$	$33.6_{\pm 11.3}$	$28.1_{\pm 9.0}$
Laplace	Strict	$44.7_{\pm 24.2}$	$33.9_{\pm 14.0}$	$30.0_{\pm 10.5}$	$27.3_{\pm 8.6}$
	Weak	$63.0_{\pm 26.1}$	$45.4_{\pm 18.3}$	$38.2_{\pm 13.0}$	$32.9_{\pm 10.6}$
Log-normal	Strict	$34.8_{\pm 13.2}$	$35.1_{\pm 17.1}$	$32.2_{\pm 5.1}$	$28.8_{\pm 4.2}$
	Weak	$40.0_{\pm 4.0}$	$37.5_{\pm 7.6}$	$33.7_{\pm 7.6}$	$30.5_{\pm 6.6}$
Gamma	Strict	$34.8_{\pm 40.4}$	$24.7_{\pm 10.5}$	$21.1_{\pm 5.7}$	$19.9_{\pm 5.4}$
	Weak	$22.2_{\pm 3.3}$	$23.7_{\pm 5.7}$	$19.0_{\pm 5.1}$	$18.6_{\pm 5.0}$
Weibull	Strict	$38.0_{\pm 13.0}$	$36.9_{\pm 9.9}$	$32.5_{\pm 7.1}$	$21.4_{\pm 0.5}$
	Weak	$45.3_{\pm 4.9}$	$39.9_{\pm 10.5}$	$33.6_{\pm 9.4}$	$23.0_{\pm 1.8}$

parameter values. In the case given in Fig. 3(d), the root being out of $[0, 1]$ is calculated by the H-R method. Such moment vectors are rarely encountered in the generated tested moment set.

6.1. Test cases for validation of the proposed method

The system of moment equations (7) for growth by using quadrature approximation, for $k \in \mathbb{N}$, can be given as

$$\frac{m_k}{dt} = -g(t,\xi)\eta(t,\xi)|_0^{\xi_{max}} + k\sum_{i=1}^{P} w_i \sum_{j=1}^{Q} \omega_j^{(\sigma)} \xi_{ij}^{k-1} g(t,\xi_{ij}), \tag{21}$$

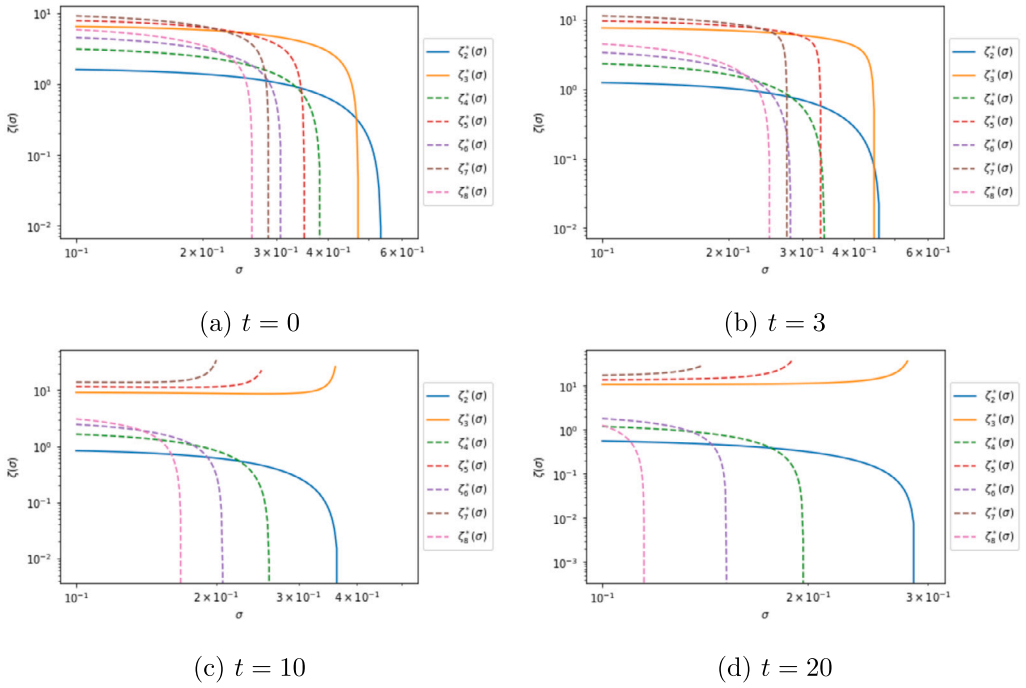

Fig. 5. Evolution of $\zeta_k^*(\sigma)$, where $k = 2, 3, 4, 5, 6, 7, 8$ for Diffusion-controlled growth with LogN KDF at $t = 0, 3, 10, 20$.

where $\xi_{ij} = \xi_i \lambda_j^{(\sigma)}$ for Gauss-Wigert and $\xi_{ij} = \sigma \lambda_j^{(\sigma)}$ for Gauss-Laguerre quadrature approximations.

The system of moment equations for aggregation by using Gauss-Wigert quadrature approximation (13), for $k \in \mathbb{N}$ can be given as

$$\frac{m_k}{dt} = \frac{1}{2} \sum_{i_1=1}^{P} \sum_{j_1=1}^{Q_{i_1}} \sum_{i_2=1}^{P} \sum_{j_2=1}^{Q_{i_2}} w_{i_1 j_1} w_{i_2 j_2} [(\xi_{i_1 j_1} + \xi_{i_2 j_2})^k - \xi_{i_1 j_1}^k - \xi_{i_2 j_2}^k] \beta(\xi_{i_1 j_1}, \xi_{i_2 j_2}), \tag{22}$$

where $\xi_{i_1 j_1} = \xi_{i_1} \lambda_{j_1}^{(\sigma)}$, $\xi_{i_2 j_2} = \xi_{i_2} \lambda_{j_2}^{(\sigma)}$, $w_{i_1 j_1} = w_{i_1} \omega_{j_1}^{(\sigma)}$ and $w_{i_2 j_2} = w_{i_2} \omega_{j_2}^{(\sigma)}$. This quadrature rule needs to be calculated for each value of σ. For each Gamma KDF, this becomes

$$\delta_\sigma(\xi, \xi_i) = \frac{\xi^{l-1} exp(-\xi/\sigma)}{\Gamma(l) \sigma^l} \tag{23}$$

with $l = \frac{\xi_i}{\sigma}$ and $\Gamma(x) = \int_0^\infty t^{x-1} e^{-t} dt$.

Similarly, the system of moment equations can be obtained by substituting Gauss-Laguerre quadrature approximation (14) in (7). This quadrature rule needs to be calculated for each value of σ. For each LogN KDF, this becomes

$$\delta_\sigma(\xi, \xi_i) = \frac{1}{\sigma \xi \sqrt{2\pi}} exp(-\frac{(\log(\xi) - \log(\xi_i))^2}{2\sigma^2}. \tag{24}$$

Case 1: Diffusion-controlled growth

A pure diffusion-controlled growth case described by McGraw [21] is considered here. In this case, the chosen internal coordinate for the size variable is radius r (μm)). The initial distribution is given by $\eta(0, r) = 0.108 e^{-0.6r}$. The growth rate is given by $R_{grow} = 2.34r$.

Using the particle radius as the interval variable, the analytic solution is given by:

$$\eta(t, r) = 0.108 r \sqrt{r^2 - \frac{2}{3} 2.34t} \exp(-b \sqrt{r^2 - \frac{2}{3} 2.34t}). \tag{25}$$

The results for the test case are presented by using the LogN KDF for $P = 3$ and Gamma KDF for $P = 4$ with the moment-inversion procedure based on Halley-Ridder (H-R) method in Fig. 4. It can be observed that the reconstructed NDFs are very similar for both LogN and Gamma KDFs, and relatively match better with the exact solution than Nguyen et al.[15]. If considering surface growth, it can be deduced from Fig. 4 that the results can be improved by using multiple moments. As seen in Fig. 4, there exists a discrepancy with the analytical solution for LogN KDF similar to the results of Nguyen et al. [15]. To explain this discrepancy, the evolution of $\zeta_2^*(\sigma)$, $\zeta_3^*(\sigma)$, …, $\zeta_8^*(\sigma)$ ($t = 0, 3, 5, 10, 20$) has been given in Fig. 5. It is observed that for $t = 0$, $\zeta_k^*(\sigma)$ functions have a root in the interval. But for $t = 20$, $k = 2, 4, 6, 8$ have a root in the interval while $k = 3, 5, 7$ do not have a root (zero at infinity). Therefore, it is presumed that this negation might be the reason for the discrepancy in Fig. 4. A similar discrepancy with the analytical solution is

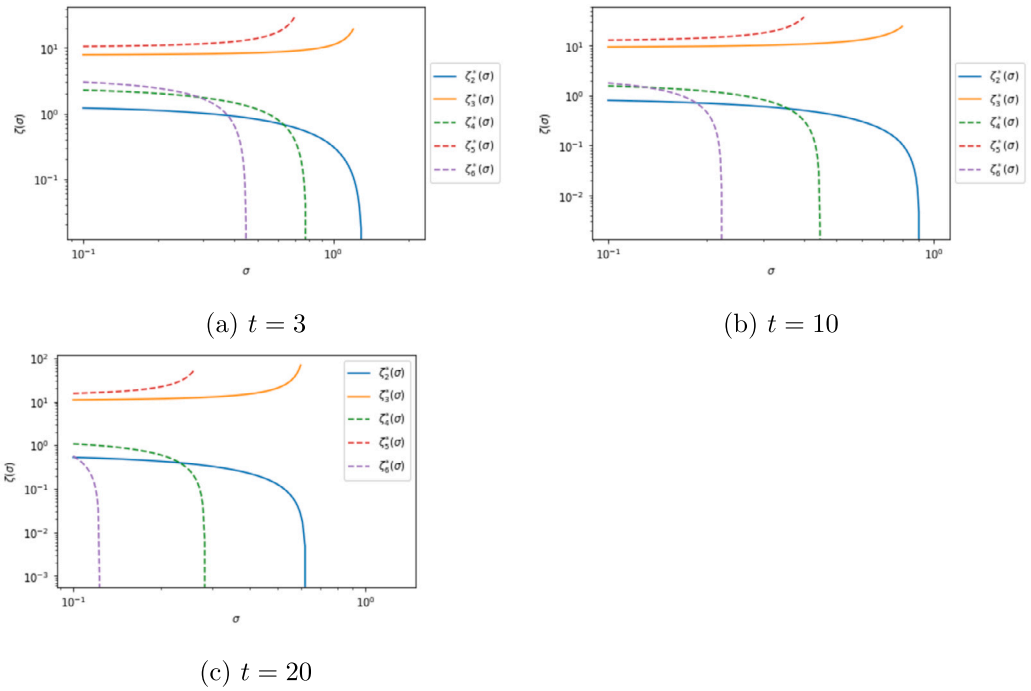

(a) $t = 3$ (b) $t = 10$

(c) $t = 20$

Fig. 6. Evolution of $\zeta_k^*(\sigma)$, where $k = 2, 3, 4, 5, 6, 7, 8$ for diffusion-controlled growth with Gamma KDF at $t = 3, 10, 20$.

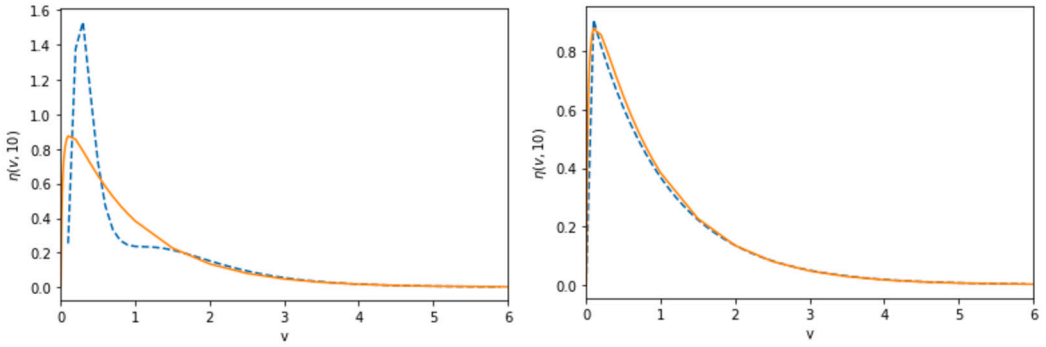

Fig. 7. Brownian aggregation with self-similar NDF (solid orange line) at $t = 10$ ($\eta(v, 10)$): LogN KDF (left) for $P = 2$ and Gamma KDF (right) for $P = 4$.

found in Nguyen et al. [15]. The evolution of $\zeta_2^*(\sigma)$, $\zeta_3^*(\sigma)$,..., $\zeta_6^*(\sigma)$ $(t = 0, 3, 10)$ is given in Fig. 6 for Gamma KDF where the same situation is observed as well.

Case 2: Aggregation with Brownian kernel

A pure aggregation case using the Brownian kernel described by von Smoluchowski [36] $\beta(v, v') = (v^{1/3} + (v')^{1/3}) \times (v^{-1/3} + (v')^{-1/3})$ is considered here. In this case, the chosen internal coordinate for the size variable is volume v. The initial condition is given by $\eta(0, v) = exp(-v)$. The results for the test case are presented by using the LogN KDF for $P = 2$ and Gamma KDF for $P = 4$ with the moment-inversion procedure based on Halley-Ridder (H-R) method in Fig. 7.

It can be observed that Gamma KDF results match better than LogN KDF results. The NDF calculated with Gamma KDF is significantly accurate and slightly better in agreement with self-similar NDF as shown in Nguyen et al. [15]. There exists a discrepancy with self-similar NDF solution for LogN KDF, similar to the results of Nguyen et al. [15]. To explain this discrepancy, the evolution of $\zeta_2^*(\sigma)$, $\zeta_3^*(\sigma)$, $\zeta_4^*(\sigma)$ $(t = 10)$ has been given in Fig. 8.

It is observed in Fig. 8 that for $t = 10$, there is $\zeta_4^*(0) = \zeta_3^*(0) > \zeta_2^*(0)$ and the difference between $\zeta_3^*(0)$ and $\zeta_2^*(0)$ values is relatively large. However for σ_P, the difference between $\zeta_3^*(\sigma_P)$ and $\zeta_2^*(\sigma_P)$ is relatively small. This causes a change in the recurring coefficients for $\mathbf{a}_{P-1}^*(\sigma)$ and $\mathbf{b}_{P-1}^*(\sigma)$ in the Jacobi matrix.

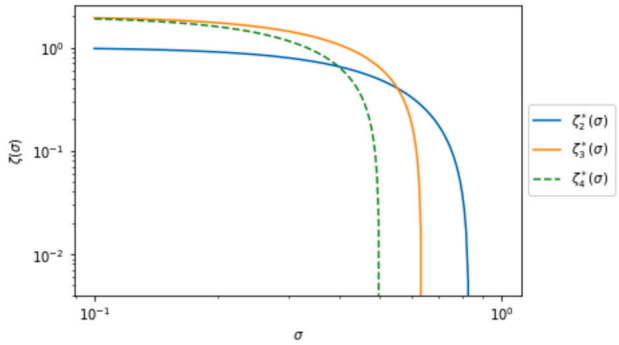

Fig. 8. Brownian aggregation with self-similar NDF (solid orange line) at $t = 10$ ($\eta(v, 10)$): LogN KDF for $P = 2$.

7. Conclusion

A moment-inversion procedure based on the proposed Halley-Ridder (H-R) method has been implemented in this study. The computation of convergence via the core-iterative procedure based on recurring coefficients namely, $b_k^*(\sigma)$, $\zeta_k^*(\sigma)$ and $\tau_k^*(\sigma)$ are mentioned for situations encountered in moment-inversion procedures. Three cases in which the procedures do not respond are examined in detail. They can be given by (i) calculation of the σ root being out of the initial interval, (ii) calculation of the smallest σ root in the case there is more than one σ_P, or there is multiple σ_P roots and (iii) for the Hausdorff problem, calculation the σ_P root when there is a gap where convergence criteria is undefined. For (iii), because the $\tau_k^*(\sigma)$ must be smaller than 1, it is hard to exceed the gap where the convergence criteria is undefined and reach the σ_P. Due to the additional condition, the H-R method responds positively to (iii). Although there is no significant improvement in the extent of variability relative to the mean of the tested shape parameter values, an increase in the number of FLOPS has been observed which the proposed procedure responds to with limitations. The total number of FLOPS for all the KDFs (Gauss, Laplace, Log-normal Gamma and Weibull) used for the EQMOM approximation in this study increased by around 30%. This indicates a more reliable and robust moment-inversion procedure for use with the quadrature-based method of moments.

CRediT authorship contribution statement

Meltem Turan: Conceptualization, Methodology, Data analysis, Writing- Original draft preparation. **Abhishek Dutta:** Data analysis, Investigation, Supervision, Writing- Reviewing and Editing

Declaration of competing interest

The authors declare that they have no known competing financial interests or personal relationships that could have appeared to influence the work reported in this paper.

Data availability

Data referenced in article.

Appendix A. Root-finding algorithms

A.1. Ridder's method

Ridder's method is an iterative root-finding algorithm [14,37] based on the false position method which is used for the calculation of the root of a real continuous function. When a root is in the range $(\vartheta_1, \vartheta_2)$, firstly the midpoint $\vartheta_3 = (\vartheta_1 + \vartheta_2)/2$ is evaluated. It then approximates the root by using an unique exponential function e^X which turns the residual function into a straight line such that it gives

$$\psi(\vartheta_1) - 2\psi(\vartheta_3)e^X + \psi(\vartheta_2)e^{2X} = 0. \tag{A.1}$$

This is a quadratic equation in e^X, whose solution is calculated from

$$e^X = \frac{\psi(\vartheta_3) + sign[\psi(\vartheta_2)]\sqrt{\psi(\vartheta_3)^2 - \psi(\vartheta_1)\psi(\vartheta_2)}}{\psi(\vartheta_2)}. \tag{A.2}$$

Then, a new guess for the root, ϑ_4 can be computed by applying the false position method, not to the values $\psi(\vartheta_1)$, $\psi(\vartheta_3)$, $\psi(\vartheta_2)$ but to the values $\psi(\vartheta_1)$, $\psi(\vartheta_3)e^X$, $\psi(\vartheta_2)e^{2X}$. The overall formula is given by:

$$\vartheta_4 = \vartheta_3 + \frac{(\vartheta_3 - \vartheta_1) sign[\psi(\vartheta_1) - \psi(\vartheta_2)]\psi(\vartheta_3)}{\psi(\vartheta_3)^2 - \psi(\vartheta_1)\psi(\vartheta_2)} \tag{A.3}$$

and it guarantees that ϑ_4 lies in the interval $(\vartheta_1, \vartheta_2)$, so ϑ_4 never moves out of the interval. Further, the convergence order of the method is $\sqrt{2}$ [37].

A.2. Halley's method

Halley's method is an iterative root-finding algorithm that is used for functions of one real variable with a continuous second derivative [20,38]. Considering the second-order Taylor series

$$\psi(\vartheta) = \psi(\vartheta_n) + \psi'(\vartheta_n)(\vartheta - \vartheta_n) + \frac{1}{2}\psi''(\vartheta_n)(\vartheta - \vartheta_n)^2 + \ldots \tag{A.4}$$

A root of $\psi(\vartheta)$ satisfies $\psi(\vartheta) = 0$, so

$$0 \approx \psi(\vartheta_n) + \psi'(\vartheta_n)(\vartheta_{n+1} - \vartheta_n) + \frac{1}{2}\psi''(\vartheta_n)(\vartheta_{n+1} - \vartheta_n)^2 + \ldots. \tag{A.5}$$

Now, reorganizing the terms yield

$$0 = \psi(\vartheta_n) + (\vartheta_{n+1} - \vartheta_n)[\psi'(\vartheta_n) + \frac{1}{2}\psi''(\vartheta_n)(\vartheta_{n+1} - \vartheta_n)^2], \tag{A.6}$$

Putting second term to left side and dividing by $\psi'(\vartheta_n) + \frac{1}{2}\psi''(\vartheta_n)(\vartheta_{n+1} - \vartheta_n)$ gives

$$\vartheta_{n+1} = \vartheta_n - \frac{\psi(\vartheta_n)}{\psi'(\vartheta_n) + \frac{1}{2}\psi''(\vartheta_n)(\vartheta_{n+1} - \vartheta_n)^2}. \tag{A.7}$$

Using the result from Newton's method,

$$\vartheta_{n+1} - \vartheta_n = -\frac{\psi(\vartheta_n)}{\psi'(\vartheta_n)}, \tag{A.8}$$

Gives

$$\vartheta_{n+1} = \vartheta_n - \frac{2\psi(\vartheta_n)\psi'(\vartheta_n)}{2[\psi'(\vartheta_n)]^2 - \psi(\vartheta_n)\psi''(\vartheta_n)}. \tag{A.9}$$

In Equation (A.9), ϑ_{n+1} is free and is not confined so the method never comes out of the interval $(\vartheta_1, \vartheta_2)$. Moreover, the convergence order of the method is 3 i.e. it converges cubically [20].

References

[1] X. Zhou, Y. Ma, M. Liu, Y. Zhang, Cfd-pbm simulations on hydrodynamics and gas-liquid mass transfer in a gas-liquid-solid circulating fluidized bed, Powder Technol. 362 (2020) 57–74.

[2] Z.-Q. Wen, X.-B. Zhang, Z.-H. Luo, Development of a coalescence model in gas–solid fluidized bed for the population balance equation, Chem. Eng. J. 440 (2022) 135904.

[3] L. Li, X. Li, Z. Zhu, B. Li, Numerical modeling of multiphase flow in gas stirred ladles: from a multiscale point of view, Powder Technol. 373 (2020) 14–25.

[4] P.B. Neto, F. Meierhofer, H.F. Meier, U. Fritsching, D. Noriler, Modelling polydisperse nanoparticle size distributions as produced via flame spray pyrolysis, Powder Technol. 370 (2020) 116–128.

[5] A. Dutta, D. Constales, G.J. Heynderickx, Applying the direct quadrature method of moments to improve multiphase fcc riser reactor simulation, Chem. Eng. Sci. 83 (2012) 93–109.

[6] T. Rosenbaum, L. Tan, M. Dummeldinger, N. Mitchell, J. Engstrom, Population balance modeling to predict particle size distribution upon scale-up of a combined antisolvent and cooling crystallization of an active pharmaceutical ingredient, Organ. Process Res. Develop. 23 (12) (2019) 2666–2677.

[7] D. Van Hauwermeiren, M. Verstraeten, P. Doshi, M.T. am Ende, N. Turnbull, K. Lee, T. De Beer, I. Nopens, On the modelling of granule size distributions in twin-screw wet granulation: calibration of a novel compartmental population balance model, Powder Technol. 341 (2019) 116–125.

[8] A. Majumder, V. Kariwala, S. Ansumali, A. Rajendran, Lattice boltzmann method for multi-dimensional population balance models in crystallization, Chem. Eng. Sci. 70 (2012) 121–134.

[9] S. Wu, S. Yang, K.L. Tay, W. Yang, M. Jia, A hybrid sectional moment projection method for discrete population balance dynamics involving inception, growth, coagulation and fragmentation, Chem. Eng. Sci. 249 (2022) 117333.

[10] A. Bouaniche, L. Vervisch, P. Domingo, A hybrid stochastic/fixed-sectional method for solving the population balance equation, Chem. Eng. Sci. 209 (2019) 115198.

[11] G. Kaur, R. Singh, H. Briesen, Approximate solutions of aggregation and breakage population balance equations, J. Math. Anal. Appl. 512 (2) (2022) 126166.

[12] M. Singh, V. Ranade, O. Shardt, T. Matsoukas, Challenges and opportunities concerning numerical solutions for population balances: a critical review, J. Phys. A, Math. Theor. 55 (38) (2022) 383002.

[13] C. Yuan, F. Laurent, R. Fox, An extended quadrature method of moments for population balance equations, J. Aerosol Sci. (ISSN 0021-8502) 51 (2012) 1–23.

[14] W. Press, S. Teukolsky, W. Vetterling, B. Flannery, Numerical Recipes: The Art of Scientific Computing, 2007.

[15] T. Nguyen, F. Laurent, R. Fox, M. Massot, Solution of population balance equations in applications with fine particles: mathematical modeling and numerical schemes, J. Comput. Phys. (ISSN 0021-9991) (325) (2016) 129–156.

[16] M. Pigou, J. Morchain, P. Fede, M. Penet, New developments of the extended quadrature method of moments to solve population balance equations, J. Comput. Phys. 365 (2018) 243–268.

[17] M. Pütz, M. Pollack, C. Hasse, M. Oevermann, A gauss/anti-gauss quadrature method of moments applied to population balance equations with turbulence-induced nonlinear phase-space diffusion, J. Comput. Phys. 466 (2022) 111363.

[18] R.O. Fox, A quadrature-based third-order moment method for dilute gas-particle flows, J. Comput. Phys. 227 (12) (2008) 6313–6350.
[19] M. Zhou, D. Bai, Y. Zong, L. Zhao, J.N. Thornock, Numerical investigation of turbulent reactive mixing in a novel coaxial jet static mixer, Chem. Eng. Process., Process Intensific. 122 (2017) 190–203.
[20] R.L. Burden, J.D. Faires, A.M. Burden, Numerical Analysis, 2000.
[21] R. McGraw, Description of aerosol dynamics by the quadrature method of moments, Aerosol Sci. Technol. 27 (2) (1997) 255–265.
[22] P. Henrici, Topics in computational complex analysis: Ii. new developments concerning the quotient-difference algorithm, in: Computational Aspects of Complex Analysis: Proceedings of the NATO Advanced Study Institute held at Braunlage, Harz, Germany, July 26–August 6, 1982, Springer, 1983, pp. 149–168.
[23] R.G. Gordon, Error bounds in equilibrium statistical mechanics, J. Math. Phys. 9 (5) (1968) 655–663.
[24] J.C. Wheeler, Modified moments and gaussian quadratures, Rocky Mt. J. Math. 4 (2) (1974) 287–296.
[25] V. John, I. Angelov, A. Öncül, D. Thévenin, Techniques for the reconstruction of a distribution from a finite number of its moments, Chem. Eng. Sci. 62 (11) (2007) 2890–2904.
[26] L.R. Mead, N. Papanicolaou, Maximum entropy in the problem of moments, J. Math. Phys. 25 (8) (1984) 2404–2417.
[27] C. Chalons, R. Fox, M. Massot, A multi-gaussian quadrature method of moments for gas-particle flows in a les framework, in: Proceedings of the Summer Program, Center for Turbulence Research, 2010, pp. 347–358.
[28] D.L. Marchisio, R.O. Fox, Computational Models for Polydisperse Particulate and Multiphase Systems, Cambridge University Press, 2013.
[29] E. Madadi-Kandjani, A. Passalacqua, An extended quadrature-based moment method with log-normal kernel density functions, Chem. Eng. Sci. 131 (2015) 323–339.
[30] W. Gautschi, Orthogonal Polynomials: Computation and Approximation, OUP, Oxford, 2004.
[31] H.M. Hulburt, S. Katz, Some problems in particle technology: a statistical mechanical formulation, Chem. Eng. Sci. 19 (8) (1964) 555–574.
[32] Z. Liu, A. Narayan, On the computation of recurrence coefficients for univariate orthogonal polynomials, J. Sci. Comput. 88 (2021) 1–26.
[33] H. Wall, Analytic Theory of Continued Fractions, 1948.
[34] J.A. Shohat, J.D. Tamarkin, The Problem of Moments, vol. 1, American Mathematical Society (RI), 1950.
[35] M. Gu, S.C. Eisenstat, A divide-and-conquer algorithm for the symmetric tridiagonal eigenproblem, SIAM J. Matrix Anal. Appl. 16 (1) (1995) 172–191.
[36] M. Von Smoluchowski, Zur kinetischen theorie der brownschen molekularbewegung und der suspensionen, Ann. Phys. 326 (14) (1906) 756–780.
[37] C. Ridders, A new algorithm for computing a single root of a real continuous function, IEEE Trans. Circuits Syst. 26 (11) (1979) 979–980.
[38] T. Scavo, J. Thoo, On the geometry of halley's method, Am. Math. Mon. 102 (5) (1995) 417–426.